Numerical simulations of void linkage in model materials using a nonlocal ductile damage approximation

Arnaud Weck, Javier Segurado, Javier LLorca, David Wilkinson, Helmut Böhm

May 13, 2008

A. Weck
McMaster University, Department of Materials Science and Engineering. 1280 Main Street West, Hamilton, ON, Canada. weckag@mcmaster.ca
J. Segurado
Universidad Politécnica de Madrid, Departamento de Ciencia de Materiales. E. T. S. de Ingenieros de Caminos, 28040 - Madrid, Spain.
J. LLorca
Universidad Politécnica de Madrid, Departamento de Ciencia de Materiales & Instituto Madrileño de Estudios Avanzados en Materiales (IMDEA-Materiales). E. T. S. de Ingenieros de Caminos, 28040 - Madrid, Spain.
D. Wilkinson
McMaster University, Department of Materials Science and Engineering. 1280 Main Street West, Hamilton, ON, Canada.
H. Böhm
Institute of Light Weight Design and Structural Biomechanics, Vienna University of Technology. Gusshausstr. 27-29, A-1040 Vienna, Austria.

Abstract

Experiments on the growth and linkage of 10 μm diameter holes laser drilled in high precision patterns into Al-plates were modelled with finite elements. The simulations used geometries identical to those of the experiments and incorporated ductile damage by element removal under the control of a ductile damage indicator based on the micromechanical studies of Rice and Tracey. A regularization of the problem was achieved through an integral-type nonlocal model based on the smoothing of the rate of a damage indicator D over a characteristic length L. The simulation does not predict the experimentally observed damage acceleration either in the case where no damage is included or when only a local damage model is used. However, the full three-dimensional simulations based on the nonlocal damage methodology do predict both the failure path and the failure strain at void linkage for almost all configurations studied. For the cases considered the critical parameter controlling the local deformations at void linkage was found to be the ratio between hole diameter and hole spacing.

1 Introduction

The ductile fracture of engineering alloys takes place by the nucleation, growth and coalescence of voids during plastic deformation. Of these three stages, coalescence is the one that governs the final failure but is, however, the least understood. Coalescence involves two somewhat distinct processes, in which the voids first change their mode of growth such that the ligament between the voids starts to collapse after which the voids actually link together. Two main types of void linkage are generally observed depending on the spatial distribution, volume fraction, strength and interface properties of the inclusions and second phases in the material. In very clean materials linkage can simply proceed by complete internal necking of the ligament between voids [1, 2, 3, 4, 5, 6]. More typically however, void linkage is triggered by

the nucleation of a second population of voids nucleated at inclusions between the primary coalescing voids. This generally occurs when the second population of inclusions has a low fracture stress or is weakly bonded to the matrix material [7, 8].

From a practical viewpoint, it is desirable to predict the failure strain of a material from information on its mechanical properties and the spatial distribution and strength of the inclusions in the microstructure. Obviously, this task is extremely complex and the early models available in the literature were successful to predict the coalescence strains only for specific materials, void configurations or stress states [9, 10, 11, 12]. More recent models [13, 14, 15, 16, 17] succeeded in predicting coalescence but at the cost of being more complicated and requiring more adjustable parameters. These parameters are generally difficult to extract from experimental data. Along with the models, a number of finite element approaches have been documented in the literature to predict ductile fracture. The progression of damage up to failure is usually introduced at a continuum level through strain softening in the constitutive response of the material. One important issue with this approach is that the results depend on the finite element discretization because localization takes place in a band one element wide [18, 19, 20]. To remove the mesh sensitivity, a characteristic length can be introduced into the constitutive model that serves to regularize the governing equations, giving rise to a nonlocal material description. Various regularization techniques have been developed [22, 23, 24, 25, 26, 27, 19], which serve as very useful and powerful tools to evaluate the progress of damage by void growth and coalescence. However, it is important to demonstrate their ability to simulate accurately the whole damage process. This is the main objective of the current investigation which relies on recent experimental results from tensile tests using model materials in which different void populations were artificially drilled in sheet samples using a femtosecond laser system [21]. These holes provide a precisely controlled population of artificial primary voids, so that the experiments enable us to capture the details of the void growth and their linkage in well defined configurations, and provide quantitative information which can be used to validate the simulations. These holes are much larger than the secondary voids that appear late in the deformation process. This enables a good correlation between the behavior of these artificial holes and the models. Note however that the damage model used in the simulations is intended to include the effect of microscale damage by the growth and coalescence of these secondary voids nucleated in the ligament between the main (laser-drilled) holes.

It should be noted here that the experimental results which are presented in detail elsewhere [21] also demonstrate the difficulty in experimentally capturing the onset of coalescence in terms a strong mode of localization in the ligament between the voids. For example coalescence is often defined to commence when voids start to grow laterally towards their neighbors. While such processes are indeed detected in the experiments the process of lateral void growth is so gradual that the point of initiation cannot be determined with any accuracy. Instead we find that only void linkage, which corresponds to the point at which the ligament between the holes is broken, can be precisely and reproducibly quantified. Therefore, in this paper, what is compared in detail is the evolution of the major axis of the primary voids and the point of complete inter-void ligament failure.

Finite element simulations of the model materials were carried out using an integral-type nonlocal ductile fracture model developed by Drabek and Böhm [20]. Damage is taken into account in this model by removing the elements in which a damage indicator, based on the micromechanical studies of Rice and Tracey [33], reaches a critical value. Regularization of the problem is achieved through an integral-type nonlocal model based on the smoothing of the rate of a damage indicator D over a characteristic length L. The results of the simulations for a given set of material parameters are compared with the experimental observations for a variety of hole configurations. It is shown that fully three-dimensional simulations can predict both the failure path and the failure strain at the point of void linkage for almost all cases and clearly outperform both damage free and local damage models.

2 Experimental results

Ductile fracture was studied experimentally in model materials created by drilling holes with a fs-pulsed laser in a 5052 Al alloy plate of 100 μm in thickness. The Al alloy composition is shown in Table 1. Samples machined from the plate had a dog-bone shape with a central section of 4 mm in length and 2 mm in width. They were placed on an X-Y translation stage which allowed for the precise positioning of the laser holes. Each hole, of 10 μm in diameter, was drilled with 1000 pulses, each of $\sim$150 fs duration and 10 μJ energy. Different configurations of holes were introduced in the central section of the dog-bone specimens. They included two holes oriented at 90° with respect to the tensile axis and spaced 15, 25, 37 and 50 μm apart and two holes oriented at 45° with respect to the tensile axis and spaced 37 μm apart. Regular arrays and random distributions of holes were also tested. The samples were annealed after laser drilling to remove the effect of the heat affected zone and the resulting microstructure consisted of equiaxed grains with an average size of $\sim$10 μm and few intermetallic particles $\sim$2 μm in diameter. More details about this experimental technique can be found elsewhere [21].

The samples were deformed in tension in-situ in a scanning electron microscope and both load and displacement were recorded during the tests. Micrographs were taken at various stages of the deformation and a sequence is shown in Figure 1 for the sample with two holes oriented at 90° with respect to the tensile axis and an initial separation of 37 μm. The length of the holes along the tensile axis, a, was measured as a function of the applied strain from these micrographs. The error in the measurements of this length from the SEM images is approximately 1 μm. We define a local deformation on the scale of the primary voids as $\varepsilon_L = \ln(a/a_0)$, where a_0 is the initial void length in the tensile direction. This can be thought of as an average local strain in the region surrounding a given void. This was obtained as a function of the far-field true strain $\varepsilon_{ff} = \ln(e_{ff} + 1)$. Here e_{ff} is the far-field engineering strain measured over the gage length of the sample (4 mm). The experimental ε_L-ε_{ff} curve is plotted in Figure 2 for the sample depicted in Figure 1. This local deformation increased linearly with the far-field strain while the deformation between the holes was homogeneous. The beginning of void coalescence (which is marked by the localization of the deformation between the holes in Figure 1(b)) was associated with an acceleration of the deformation which led very rapidly to the linkage of the holes by the final fracture of the ligament between the holes, Figure 1(d). Thus, the ε_L-ε_{ff} curves are a good indicator of the ductile fracture process and will be used to compare the numerical predictions with the experimental data. The corresponding curves for the other hole configurations are presented in section 5 along with the finite element results.

Table 1: Chemical composition of the 5052 Al-Mg alloy.

Si	Fe	Cu	Mn	Mg	Cr	Zn	Ti	Other	Al
0.25	0.40	0.10	0.10	2.50	0.15	0.10	0.05	0.015	Rem.

The fracture surface of a sample containing a regular array of holes oriented 90° with respect to the tensile axis is shown in Figure 3. One can see that failure proceeded first by internal necking of the ligament between the holes, and then by the linkage of secondary voids, probably nucleated at intermetallic particles.

3 Finite element model

The ductile fracture process in samples containing holes was simulated through the finite element method. Due to the geometry of the problem, simulations were carried out using a generalized plane strain (2D) model or a full three-dimensional model. The 3D analysis takes into account the variations in strain through the thickness, although it is computationally very expensive. The 2D generalized plane strain model is an alternative in which the constant through-thickness displacement is defined for all the sample using only 3 extra degrees of freedom. The validity of using one strategy over the other will be established throughout the paper.

The element deletion technique was used to model

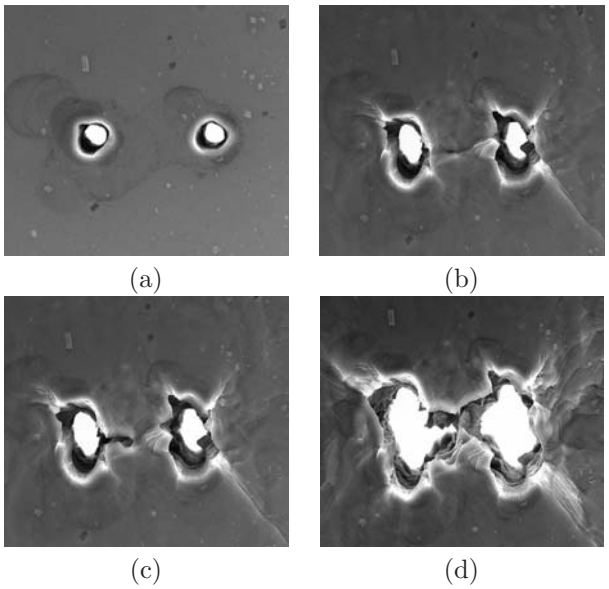

(a) (b)

(c) (d)

Figure 1: Scanning electron micrographs obtained *in situ* during the tensile deformation of the 5052 Al alloy sample with two holes oriented at 90° with respect to the tensile axis (vertical) and 37 μm apart. The far-field true strain,ε_{ff}, for each micrograph was: (a) 0.0, (b) 0.204, (c) 0.213 and (d) 0.220. This last micrograph corresponds to the instant of void linkage as the intervoid ligament is broken.

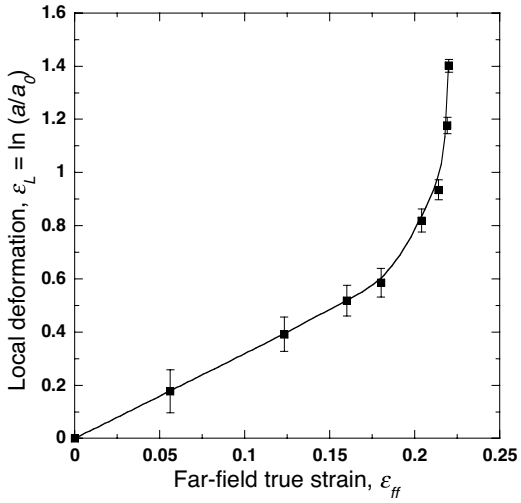

Figure 2: Experimental result showing the evolution of the local deformation at the scale of the holes, ε_L, as a function the far-field true strain, ε_{ff}, for the sample depicted in figure 1.

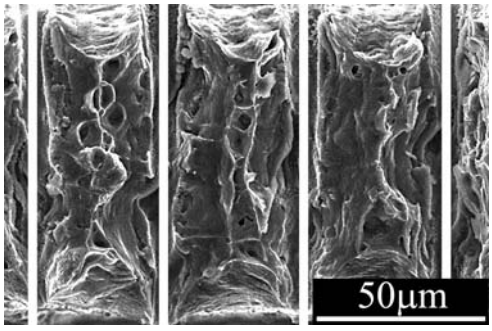

Figure 3: Fracture surface of a sample containing a regular array of holes oriented 90° with respect to the tensile axis. The sample fails by internal necking and the coalescence of secondary voids between the main laser drilled holes. The vertical white lines indicate the locations of the laser drilled holes.

damage, as will be shown below, and it was beneficial to use as many elements as possible in the simulations. Simulations were carried out with Abaqus/Standard [37] within the framework of the finite deformation theory with the initial unstressed state as reference. Generalized plane strain, 4-node bilinear quadratic elements with integration at 4 Gauss points (CPEG4) were chosen for the 2D simulations and linear 8-node brick elements with full integration (C3D8) for the 3D simulations. The Al alloy was modelled as an isotropic, elasto-plastic solid following the J_2 theory of plasticity with isotropic hardening. The elastic constants were E=70 GPa and $\nu = 0.33$, and the flow stress, $\bar{\sigma}$, was treated as a function of the accumulated plastic strain, ε_p, according to the Voce equation

$$\bar{\sigma} = A - B\exp\{-C\varepsilon_p\} \tag{1}$$

which has already been successfully used by Duan *et al.* [38] for a similar Al alloy (5754). The parameters of the Voce equation were obtained by fitting the experimental stress-strain curve obtained on a sample without holes and are given by $A = 445$ MPa, $B = 300$ MPa and $C = 5.4$.

In the context of the experiments to be modelled, ductile damage requires the presence of a population of secondary voids that are much smaller than the laser drilled primary voids. As stated in section 2 and shown in Figure 3 at least a certain number of such secondary voids were present in the samples. Due to the small size of these voids their effects were described by homogenized models. These may take the form of ductile damage models that track the evolution of the volume fraction of the secondary voids and take into account the resulting progressive loss of stress carrying capacity of the homogenized material [40, 41, 42, 43, 44]. Alternatively, models may be based on element removal controlled by a ductile damage indicator, which registers local ductile failure but does not allow to follow the degradation of the material properties prior to this point. A number of ductile damage indicators, mainly empirical, have been proposed in the literature and they are generally based on the attainment of a critical stress or strain, often incorporating the effect of stress triaxiality [9, 28, 29, 30, 31, 32]. One of the most commonly used is that proposed by Gunawardena [32] which is built upon the micromechanical model of Rice and Tracey [33] and Hancock and Mackenzie [34]. A reference failure strain, ε_f, is defined from the analysis of the growth of a spherical void in a rigid-plastic material subjected to different levels of stress triaxiality,

$$\varepsilon_f = \varepsilon_0 \exp\left(\frac{1}{2} - \frac{3}{2}\frac{\sigma_h}{\sigma_{eq}}\right) \tag{2}$$

where σ_h is the hydrostatic stress component, σ_{eq} the equivalent von Mises stress and ε_0 the failure strain in uniaxial tension. The increment of the damage indicator $\mathrm{d}D$ is then defined as

$$\mathrm{d}D = \frac{\mathrm{d}\varepsilon_p}{\varepsilon_f} \tag{3}$$

and therefore D at any material point can be computed by integrating equation (3) along the loading path, leading to

$$D = \frac{1}{\varepsilon_0}\int_0^{\varepsilon_p^c} \exp\left(\frac{3}{2}\frac{\sigma_h}{\sigma_{eq}} - \frac{1}{2}\right)\mathrm{d}\varepsilon_p \ . \tag{4}$$

where ε_p^c is the current equivalent plastic strain. Failure is indicated when D reaches unity, i.e., $D(\varepsilon_f) = 1$. After each load increment the value of the ductile damage indicator is updated at each integration point and elements are deleted if $D \geq 1$ in two or more of their integration points. Even though the algorithm based on equation 4 and element removal does not constitute a fully coupled damage model, it has the advantage of requiring only one material parameter, ε_0, which also can be directly interpreted physically.

In order to avoid mesh dependence of the numerical results, the above algorithm is coupled with a nonlocal averaging of the damage indicator. The nonlocal strategy is briefly explained here and the reader is referred to Drabek [35] for a complete description of its implementation in the finite element code Abaqus. The rate of the nonlocal damage indicator $\dot{D}_{nl}$ is expressed as a function of the local damage indicator $\dot{D}_l$ by convoluting it with a delocalization function as proposed by Leblond *et al.* [36] in the context of a Gurson-type damage model:

$$\dot{D}_{nl}(\boldsymbol{x}) = \frac{1}{W(\boldsymbol{x})}\int_V \dot{D}_l(\boldsymbol{y}) w(\boldsymbol{x}, \boldsymbol{y}, L)\mathrm{d}V \tag{5}$$

where $\boldsymbol{x}$ stands for the position vector of the point at which the nonlocal damage indicator is evaluated and $\boldsymbol{y}$ for the positions of the adjacent material points. The normalizing factor $W(\boldsymbol{x})$ is defined as

$$W(\boldsymbol{x}) = \int_V w(\boldsymbol{x}, \boldsymbol{y}, L) \mathrm{d}V \tag{6}$$

and $w(\boldsymbol{x}, \boldsymbol{y}, L)$ is a smoothing function whose form was proposed by Leblond *et al.* [36] as

$$w(\boldsymbol{x}, \boldsymbol{y}, L) = \left[\frac{1}{1 + \left(\frac{\|\boldsymbol{x}-\boldsymbol{y}\|}{L} \right)^8} \right]^2 \tag{7}$$

Spurious diffusion effects of the type reported by Enakoutsa et al. [44] for a nonlocal Gurson model were not encountered due to the different structure of the equations governing the evolution of the nonlocal variable.

4 Parameter identification for the ductile damage model

The nonlocal ductile fracture approximation described above is based upon two parameters which depend on the material, namely ε_0 (which represents the local failure strain in uniaxial tension) and the characteristic length L which intervenes in the nonlocal averaging scheme in equation (7). The point at which damage starts to accumulate in the material is controlled by ε_0 (also known as the Rice-Tracey parameter in the literature) while L limits the local gradients of the damage indicator which influences the rate at which damage evolves. For the local version of the Rice-Tracey damage indicator a procedure for calibrating the parameter ε_0 has been published [45]. However, ε_0 and L are coupled, i.e. when the characteristic length increases, damage is averaged over a larger area and thus ε_0 has to be reduced accordingly to obtain the same behavior. In this paper, the optimum value of these parameters was determined by fitting to the experimental results of the sample containing 2 holes oriented at 90° with respect to the tensile axis and spaced 37 μm apart (Figure 2).

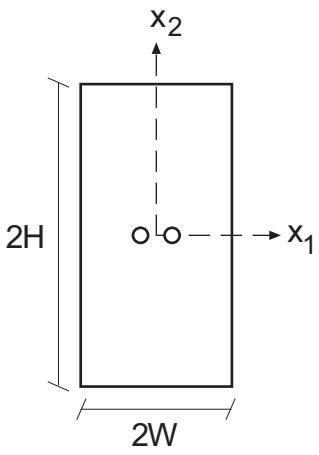

Figure 4: Schematic of the sample for the simulations for the model with two holes oriented at 90° with respect to the tensile axis and spaced 37 μm. Drawing not to scale.

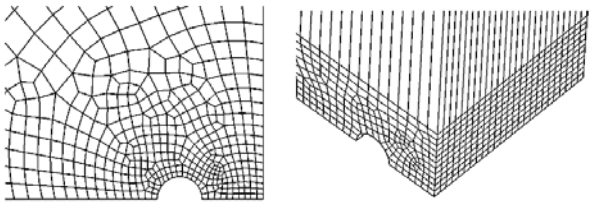

Figure 5: Details of the finite element discretization (in two and three dimensions) of the sample with 2 holes oriented at 90° with respect to the tensile axis.

The analysis simulates the behavior in uniaxial tension of the central section of $2W$ x $2H$ x $2t$ (2 x 4 x 0.1 mm^3) of the dog-bone specimen with two holes (Figure 4). Due to the mirror symmetries of the problem, only 1/8th of the sample has to be discretized with three planes of symmetry located at $x_1 = 0$, $x_2 = 0$ and $x_3 = 0$. Tensile deformation is imposed by applying a uniform displacement in the x_2 direction to the upper surface of the sample ($x_2 = H$), while the lateral surfaces ($x_1 = W$ and $x_3 = t$) remained stress-free. A detail of the finite element discretization is shown in Figure 5.

The first set of simulations analyzed the influence

of the characteristic length L on the mechanical response for a fixed value of $\varepsilon_0 = 0.4$. The numerical predictions are compared with the experimental behavior through the evolution of the local deformation, $\ln(a/a_0)$, as a function of the far-field true strain, ε_{ff} in Figure 6(a). One can see that in the absence of damage, the simulation is not able to predict the failure strain controlled by the sudden localization of the deformation between the holes due to the coalescence of secondary voids. The simulation with $L = 0$, which corresponds to a local damage indicator model, is also unable to predict this behavior for the mesh used. Better results were obtained if L was increased, and the far-field strain at void linkage was adequately predicted by the non-local model with $L = 10$ μm. The influence of the reference failure strain, ε_0, is plotted in Figure 6(b). ε_0 controls the onset of damage and the optimum value to predict the experimental curve was found to be 0.4. This parameter, together with $L = 10$ μm, gives a good prediction of the failure strain but it cannot capture with accuracy the progressive acceleration of void growth observed experimentally. This is because the damage indicator triggers sudden element elimination when $D = 1$ and there is therefore no progressive unloading as damage progresses.

The propagation of damage in the simulations with ε_0=0.4 and L=10 μm is shown in the contour plots of Figure 7. The stress concentration at the sides of the hole (Figure 7(a)) leads to the initiation of damage, as shown by the white areas in Figure 7(b). These white areas represent the elements which have been removed from the analysis as they reached the critical condition for failure. Damage grows very quickly beyond this point, leading to the immediate failure of the ligament through the thickness of the sample, as shown in Figure 7(c).

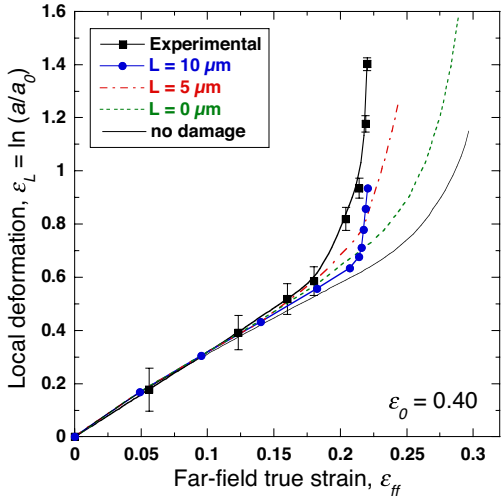

(a)

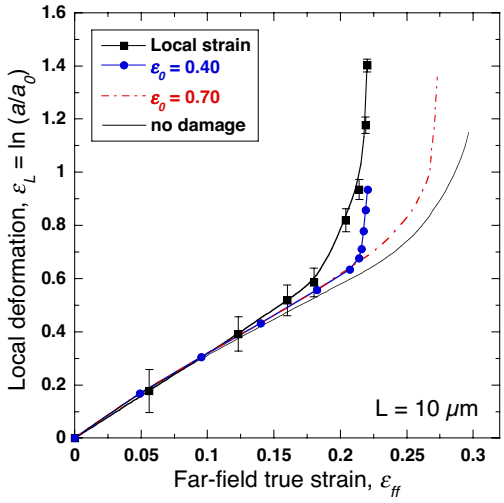

(b)

Figure 6: Identification of the simulation parameters by comparison with the experimental results on the samples with two holes oriented at 90° with respect to the tensile axis and spaced 37 μm. (a) Effect of the characteristic length L. (b) Effect of the reference failure strain, ε_0.

5 Comparison with experimental results

The simple nonlocal ductile fracture model presented above will be validated in this section by comparing the model predictions for void linkage with the ex-

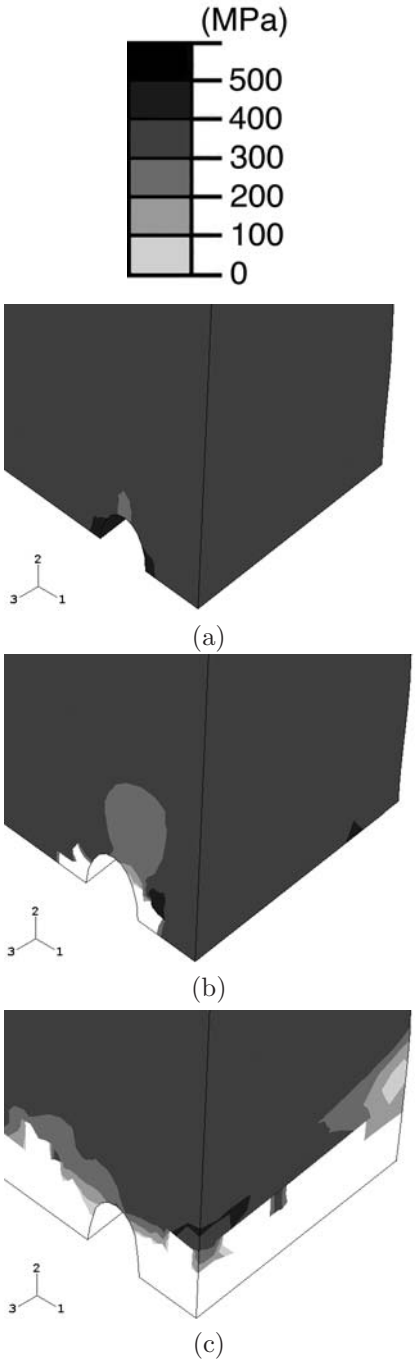

Figure 7: Contour plots of the Von Mises equivalent stress at different stages of deformation in the samples with two holes oriented at 90° with respect to the tensile axis and spaced 37 μm. The simulations were carried out with $\varepsilon_0 = 0.4$ and $L = 10$ μm. (a) ε_{ff}= 8 0.204, (b) ε_{ff}= 0.213 and (c) $\varepsilon_{ff} = 0.220$. The white regions correspond to the elements which have been deleted from the finite element mesh due to damage.

perimental results in samples with different arrangements of holes. The two parameters in the model which provided the best fit in the particular case presented in section 4, $\varepsilon_0 = 0.4$ and $L = 10$ μm, have been used in all the subsequent simulations presented below. In addition, the size of the finite elements around the holes in all the simulations was kept approximately constant and smaller than $L/3$, so that there were always at least three elements within the characteristic length L.

5.1 Effect of the hole orientation

The influence of the orientation of pairs of primary voids on the ligament failure strain was studied by placing the holes 37 μm apart but at 45° with respect to the tensile axis. Due to lower symmetry of this problem, one half of the sample was discretized and simulated numerically. The numerical predictions are compared with the experimental behavior through the evolution of the local deformation, $\ln(a/a_0)$, as a function of the far-field true strain, ε_{ff} (see Figure 8). As expected, the experimental data showed that the growth of the holes in this configuration was slower than in the sample with the holes perpendicular to the tensile axis and the failure strain was larger. The numerical simulations were in reasonably good agreement with the experimental data and the overall predictions for the far-field strain at void linkage were only slightly lower (7%) than the actual one. This agreement is remarkable because the dominant failure mechanism for this hole configuration was shear [21] and the ductile fracture model implemented is based on a mechanism of void growth at high stress triaxiality.

5.2 Effect of hole spacing

Experiments were carried out with two holes oriented at 90° with respect to the tensile axis and spaced 15, 25, 40 and 50 μm apart to study the effect of the distance between holes on void linkage. The corresponding numerical simulations were carried out in two and three-dimensions for this particular hole configuration to assess the validity and limitations of 2D models in simulating this problem. Two representa-

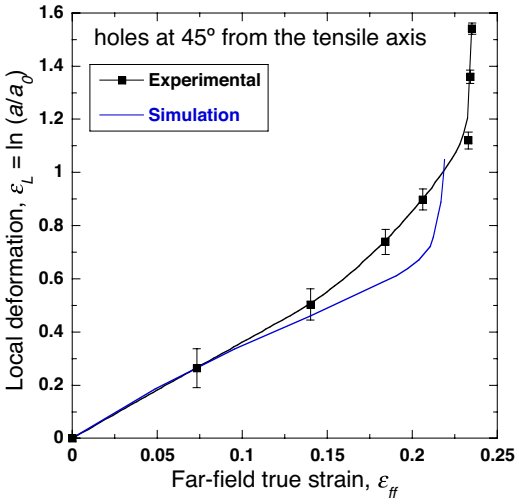

Figure 8: Experimental and numerical results of the evolution of the local deformation at the scale of the holes, ε_L, as a function the far-field true strain, ε_{ff}, for the sample with two holes orientated at 45° to the tensile axis and spaced 37 μm.

tive examples of the finite element meshes are found in Figure 5.

The experimental results and the simulations are compared in terms of the evolution the local deformation, $\ln(a/a_0)$, as a function of the far-field true strain, ε_{ff} in Figures 9(a), (b), (c) and (d) for the samples with two holes spaced at 15, 25, 40 and 50 μm, respectively. In both simulations and experiments, the far-field strain at which void linkage occurred is given in the Figure. In general, both the 2D and 3D models provide a good prediction of the far-field strain at the point of ligament failure. Moreover, the three-dimensional simulations are also accurate after coalescence begins in reproducing the fast growth of the holes during the final stage of fracture. The two-dimensional model, however, was only able to reproduce the process of damage localization in the intervoid region after the onset of damage when the distance between the holes was small. The error in this region increased rapidly with the intervoid spacing because the stress state in this region changed from plane strain to plane stress as the intervoid distance increased. Thomason [39] proposed that a plane strain condition between primary voids is fulfilled when the thickness $2t$ is at least five times the hole spacing. For the particular samples analyzed here (thickness of 100 μm and hole diameter of 10 μm), this condition was met when the hole spacing was 15 and 25 μm (Figure 9(a-d)), but not in the other two cases. Furthermore, because the generalized plane strain simulations (2D simulation) used the same displacement in the thickness direction for the whole model, the local thickness changes in the ligament between the holes cannot be captured.

5.3 Effect of spatial distribution of holes: regular array

Experiments were carried out in samples containing a regular array of holes to verify whether the failure strain is affected by the number of holes in the array and whether the nonlocal ductile damage model can also predict the behavior under such conditions. These samples contained lines with of 13 holes spaced 40 μm apart perpendicular to the tensile axis and either 1, 3 or 13 of these lines spaced 40 μm apart along

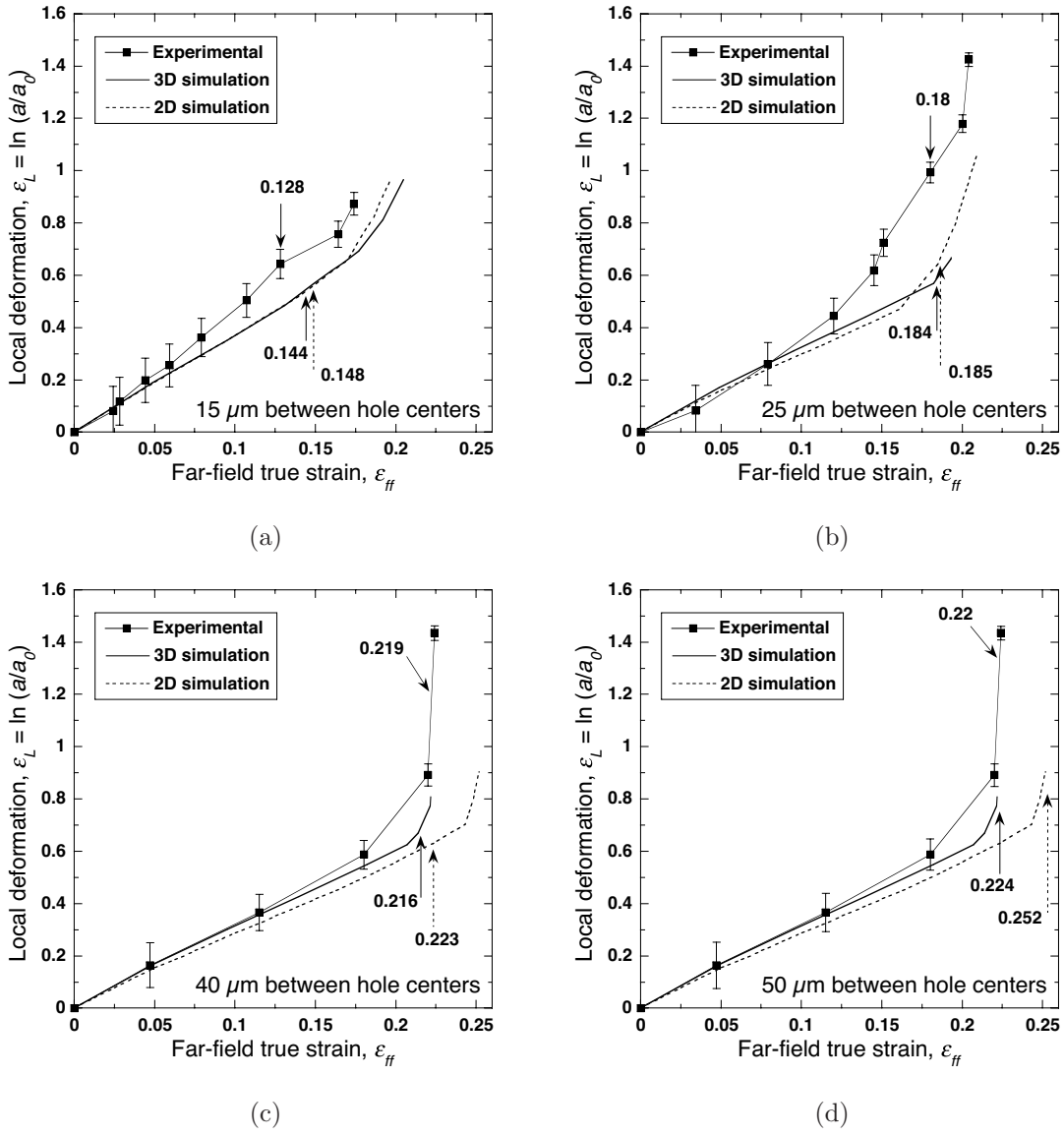

Figure 9: Experimental and numerical results of the influence of holes spacing on void linkage in the sample with two holes oriented at 90° to the tensile axis. The evolution of the local deformation at the scale of the holes, ε_L, is plotted as a function the far-field true strain, ε_{ff}. The holes spacing was (a) 15 μm, (b) 25 μm, (c) 40 μm and (d) 50 μm. The arrows and the numbers stand for the far-field strains at void linkage.

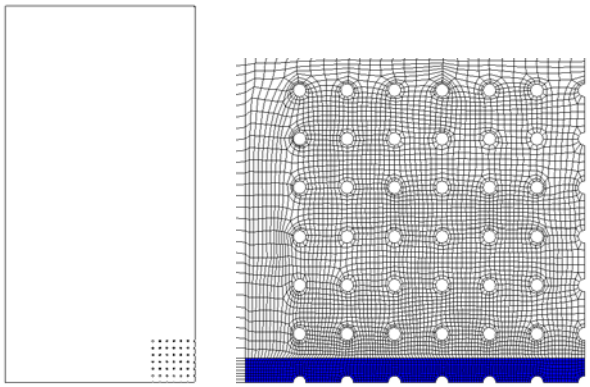

(a) (b)

Figure 10: (a) Feature edges of the finite element model used to investigate the effect of regular arrays of holes on void linkage. (b) Detail of the finite element mesh in the hole region showing in dark the zone in which the nonlocal ductile damage model was included in the simulations.

the tensile direction. These were tested until failure. The three-dimensional finite element model analyzed 1/8th of the sample due to the symmetry (Figure 10) while the boundary conditions were equivalent to those described for Figure 4. In order to save computer time, the nonlocal averaging was only carried out on a single row of holes, shown in dark in Figure 10 because the experimental data indicated that failure occurred in the middle of the array.

As in the previous cases, numerical simulations and experimental results are compared (see Figure 11) through the evolution of the local deformation on the scale of the holes, ε_L, with the far-field true strain, ε_{ff}. The critical far-field strain for void linkage increased with the number of lines of holes and the numerical model captured not only this trend but also the magnitude of the far-field strain at which void linkage occurred. These predictions strongly substantiate the validity of the simulation approach and support its use in understanding the effect of regular arrays of holes on the ductile fracture process. The maximum value of the von Mises equivalent stress between the holes is shown in Table 2 along with the length of the holes a for the three arrays of holes analyzed when the applied far-field strain was 14.8%. The maximum equivalent stress between the holes and the elongation of the primary voids decreased with the number of lines of holes because each line of holes contributes to the overall longitudinal elongation of the sample. Thus plasticity was spread out whereas it is much more localized if there is only one line of holes. It can be concluded from these results that the number of lines of holes in the tensile direction modifies the far-field strain at the linkage event but not the local magnitude of the strain at which linkage occurs. This is in agreement with Figure 11 which shows that the local deformation at void linkage (represented by horizontal dashed line) is independent of the number of void lines.

Table 2: Maximum Von Mises equivalent stress, σ_{eq}, between the holes and hole length along the tensile axis, a, as a function of the number of lines of holes at $\varepsilon_{ff} = 14.8\%$.

Lines of holes	σ_{eq} [MPa]	a [μm]
1	432	9.06
3	427	8.33
13	410	7.72

5.4 Effect of spatial distribution of holes: random array

Regular arrays of holes are not frequent in engineering materials, and so random distributions are of more technological interest. A sample with a random array of holes was machined and the corresponding finite element mesh is shown in Figure 12. One half of the sample has to be discretized and analyzed because, as in the sample with the holes oriented at 45°, the only plane of symmetry is $x_3 = 0$. As in the previous simulations, and in order to conserve computational time, the nonlocal failure model was restricted to the dark area in Figure 12 in which failure was observed experimentally.

The evolution of the local deformation at the scale of the primary voids, obtained from the finite element analyses, ε_L, is plotted in Figure 13 versus the

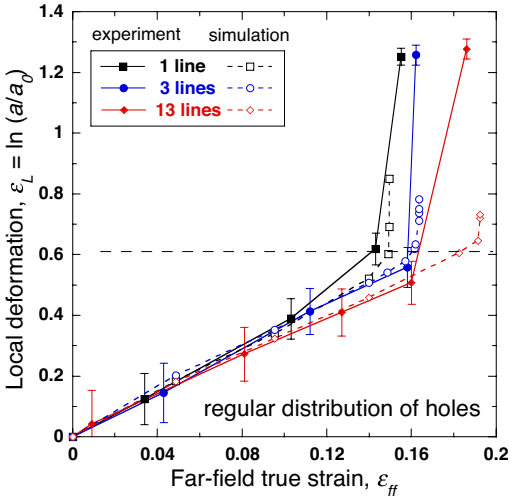

Figure 11: Numerical and experimental results on the evolution of the local deformation at the scale of the holes, ε_L, is plotted as a function the far-field true strain, ε_{ff} in samples with 1, 3, and 13 lines of holes along the tensile axis.

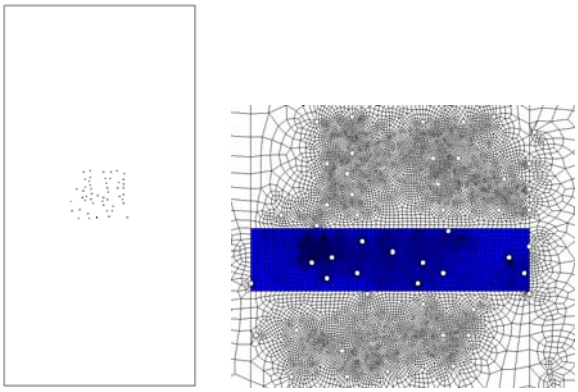

Figure 12: (a) Feature edges of the finite element model used to investigate void linkage in a random array of holes. (b) Detail of the finite element mesh in the hole region showing in dark the zone in which the nonlocal ductile damage model was included in the simulations.

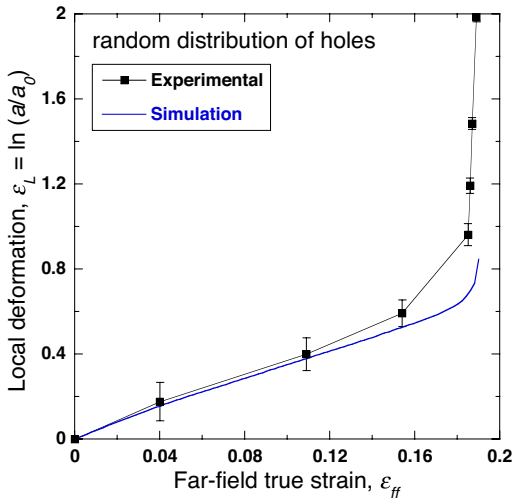

Figure 13: Numerical and experimental results on the evolution of the local deformation at the scale of the holes, ε_L, plotted as a function the far-field true strain, ε_{ff} in the sample with a random array of holes.

far-field true strain, ε_{ff}, along with the experimental results. The predictions of the fracture path through void linkage and the actual result are shown in Figures 14 and 15. It is obvious from these Figures that the numerical predictions at the macroscopic level (far-field strain at void linkage) and microscopic level (fracture path and plastic strain) are excellent, and support the ability of this simple nonlocal ductile failure model to simulate the process of void linkage under different scenarios. It should also be noted that the strong lateral void growth seen in Figure 15 is part of the void coalescence process and is therefore also accounted for in the simulation through element deletion as seen in Figures 14.

6 Discussion and conclusions

To the knowledge of the authors the present study is the first that combines experimental work with simulations of growth and linkage of primary voids in a

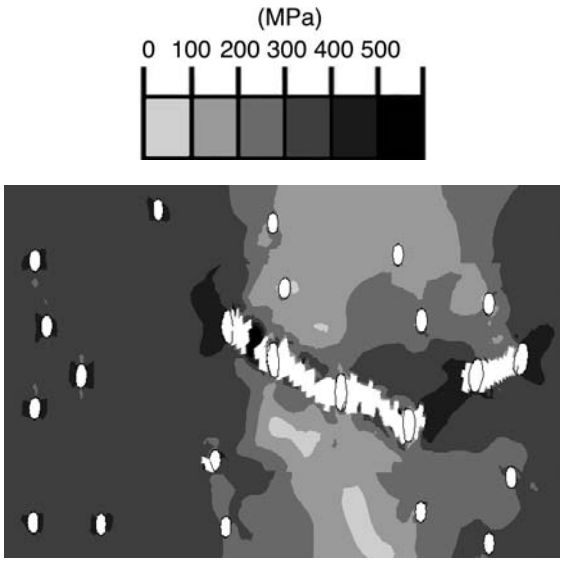

(a)

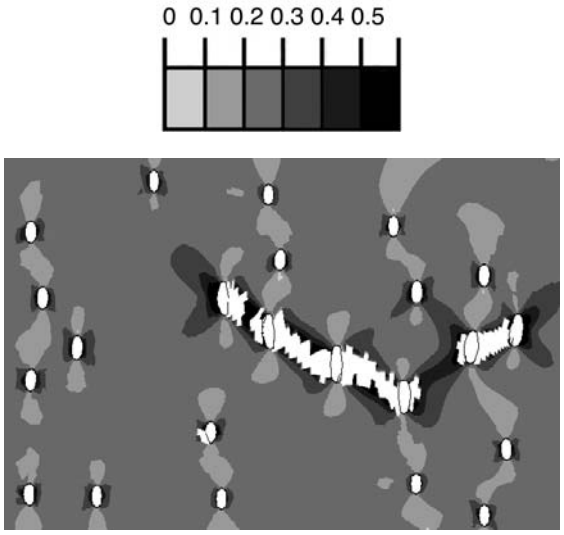

(b)

Figure 14: Numerical simulation of the fracture path after void linkage in the sample with a random array of holes. (a) Contour plot of the Von Mises equivalent stress. The white regions correspond to the elements which have been deleted from the finite element mesh due to damage. (b) *Idem* as (a) but the contour plot shows the accumulated plastic strain.

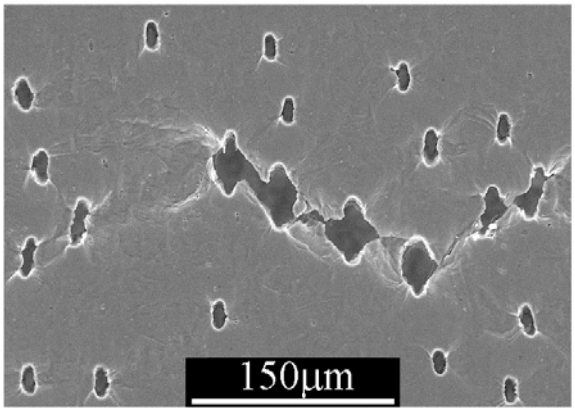

Figure 15: Micrograph of the fracture path after void linkage in the sample with a random array of holes.

ductile material on the basis of specimens that contain patterns of holes of precisely defined size and position. For the simulations a simple but robust model was used that employs a nonlocal version of the damage indicator proposed by Gunawardena et al. [32] to control element removal. This nonlocal model has only two adjustable parameters, the strain at failure under uniaxial loading and a characteristic length, so that material identification is not overly complex. The application of a homogenized model for describing ductile damage rests on the assumption that a population of small secondary voids is present in the aluminum matrix, which the experiments indicate to be fulfilled. We observed that ε_0 controls the onset of secondary damage (between the primary voids) while the characteristic length L, serves to delay the onset of secondary damage to higher strains and accelerate damage evolution once it has started.

It should be emphasized that even though the model presented here has the disadvantage of not being fully coupled (like the Gurson model) it has the advantage of having only one free parameter in its local version and two in its nonlocal one. This results in a simpler model whose parameters can be easily identified from the experiments.

With a fixed set of material parameters ε_0=0.4 and L=10 μm, the nonlocal numerical simulations of damage in 3D were found to be in good agree-

ment with the experimental values of far-field strain at void linkage. These predictions were obtained with different configurations of holes including variations in the spacing between holes, as well as regular and random distributions of holes. The only discrepancy was found in the simulation of holes oriented at 45° to the tensile axis and this is very likely due to the fact that the ductile damage indicator of Rice and Tracey was developed for void growth under triaxial stresses and not for shear. Nevertheless, the differences in the strain at void linkage were limited (about 7%). This helps to explain the good results in the simulation of void linkage for a random array of holes. It is certainly clear that the simulations do not accurately capture the localization of the strain between the holes during the early part of the void linkage process because in in this modelling strategy the elements are either damage-free or fractured.

The numerical simulations also showed that using the model without damage or using only the local version of the model (in which the characteristic length $L = 0$) it was impossible to capture void growth acceleration for the mesh used and therefore the failure strains were not well predicted. However, the nonlocal version of the model proved to be clearly superior to both the local version of the Rice-Tracey damage indicator and to the damage-free model in predicting the experimentally observed behavior. Accordingly, we found that the nonlocal model is not only necessary for controlling the mesh sensitivity of the numerical solutions, but for the configurations considered, it also clearly improves the agreement between simulations and experiments. It should be noted that because the characteristic length found in this study is equal to the void diameter, it essentially imposes the use of a nonlocal modelling approach to reasonably resolve geometrical features of the size of the characteristic length such as the voids. This is hardly possible if the element size is used to introduce the characteristic length into the analysis.

The numerical simulations showed that for the constant hole diameter used in this study, the void linkage strain is mainly controlled by the distance between the holes and that the number of holes has no significant effect on the local deformation at void linkage. This is in agreement with modelling results in the literature which show the importance of the void diameter to void spacing ratio on fracture [4, 14]. Indeed, it was possible to model very different hole configurations using the same failure criterion, and this implies that the local conditions at linkage are equivalent. This also means that the differences in far-field strains at void linkage must be related to the boundary conditions while the spatial distribution of the holes controls the instant at which these critical conditions are attained at the local level.

In addition, two-dimensional simulations under generalized plane strain conditions provided acceptable results when the spacing between holes is small enough, so that the ligament between holes is mainly under plane strain conditions. The stress state between the holes departs from plane strain conditions and moves towards plane stress as the intervoid distance increases, and the two-dimensional simulations can no longer predict the failure path and the failure strains. Only fully three-dimensional simulations can predict both the failure path and the failure strains for almost all configurations.

The nonlocal simulations incorporate one additional parameter, the characteristic length L, whose role is to reduce mesh sensitivity but whose relation to the physical characteristics of the material or the specimen is unclear. In fact, there are not many physically-based strategies in the literature to select the magnitude of L although it is sometimes taken to be of the order of the distance over which microstructural features have an effect. For the configurations considered good results were obtained by setting the characteristic length equal to the diameter of the primary voids, which also corresponds to the average size of the grains in the aluminum matrix. This does not imply, however, that the diameter of primary voids or inhomogeneities is always a valid choice for the characteristic length for ductile damage.

The combination of nonlocal models with experiments on samples that contain precise two- and three-dimensional patterns of primary voids can provide a fruitful path towards obtaining a deeper understanding of the role of the characteristic length in ductile damage and towards improved insight into the growth and linkage of voids in ductile materials.

Acknowledgement

We acknowledge the financial support from the Comunidad de Madrid through the program ESTRUMAT-CM, the Ministerio de Educación y Ciencia de España through grant MAT2006-2602 and the Natural Sciences and Engineering Research Council of Canada (NSERC).

References

[1] Thompson, A.W. (1987) Modeling of local strains in ductile fracture, Metallurgical Transactions A, 18A:1877-1886

[2] Puttick, K. E. (1959) Ductile Fracture in Metals, Philosophical Magazine, 4:964-969

[3] Knott, J.F. (1980) Micromechanisms of fibrous crack extension in engineering alloys, Metal Science, 14:327-336

[4] Benzerga, A.A. and Besson, J. and Pineau, A. (2004) Anisotropic ductile fracture Part I: experiments, Acta Materialia, 52:4623-4638

[5] Park, In-Gyu and Thompson, Anthony W. (1988) Ductile fracture in spheroidized 1520 steel, Acta Metallurgica, 7:1653-1664

[6] Le Roy, G. (1978) Large Scale Plastic Deformation and Fracture for Multiaxial Stress States, Ph.D. thesis, McMaster University

[7] Cox, T. B. and Low, J. R. Jr. (1974) Investigation of the Plastic Fracture of AISI 4340 and 18 Nickel-200 Grade Maraging Steels, Metallurgical Transactions, 5:1457-1470, 1974

[8] Marini, B. and Mudry, F. and Pineau, A. (1985) Experimental study of cavity growth in ductile rupture, Engineering Fracture Mechanics, 22:989-996

[9] McClintock, F.A. (1968) Criterion for ductile fracture by the growth of holes., Journal of Applied Mechanics, 35:363-371

[10] Brown, M. and Embury, D. (1973) The Initiation and growth of voids at second phase particles., Third International Conference on the Strength of Metals and Alloys, Institute of Metals, London, 168-164

[11] Needleman, A. and Tvergaard, V. (1984) An analysis of ductile rupture in notched bars, Journal of the Mechanics and Physics of Solids, 32:461-490

[12] Thomason, P.F. (1968) A theory for ductile fracture by internal necking of cavities, Journal of the Institute of Metals, 96:360-365

[13] Zhang, Z.L. and Niemi, E. (1994) A new failure criterion for the Gurson-Tvergaard dilational constitutive model, International Journal of Fracture, 70:321-334

[14] Pardoen, T. and Hutchinson, J.W. (2000) An extended model for void growth and coalescence, Journal of the Mechanics and Physics of Solids, 48:2467-2512

[15] Gologanu, M. and Leblond, J.-B. and Perrin, G. and Devaux, J. (2001) Theoretical models for void coalescence in porous ductile solids. I. Coalescence "in layers", International Journal of Solids and Structures, 38:5581-5594

[16] Gologanu, M. and Leblond, J.-B. and Devaux, J. (2001) Theoretical models for void coalescence in porous ductile solids. II. Coalescence "in columns", International Journal of Solids and Structures, 38:5595-5604

[17] Benzerga, A.A. (2002) Micromechanics of coalescence in ductile fracture, Journal of the Mechanics and Physics of Solids, 50:1331-1362,

[18] Pijaudier-Cabot, G. and Mazars, J. and Pulikowski, J. (1991) Steel-Concrete Bond Analysis with Nonlocal Continuous Damage, Journal of Structural Engineering-ASCE, 117:862-882

[19] de Borst, R. (1991) Simulation of Strain Localization: A Reappraisal of Cosserat Continuum, Engineering Computations, 8:317-332

[20] Drabek, T. and Böhm, H.J. (2005) Damage models for studying ductile matrix failure in composites, Computational Materials Science, 32:329-336

[21] Weck, A. and Wilkinson, D.S. (2007) Experimental investigation of void coalescence in metallic sheets containing laser drilled holes, Submitted for publication in Acta Materialia

[22] Tvergaard, V. and Needleman, A. (1995) Effects of nonlocal damage in porous plastic solids, International Journal of Solids and Structures, 32:1063-1077

[23] Baaser, H. and Tvergaard, V. (2003) A new algorithmic approach treating nonlocal effects at finite rate-independent deformation using the Rousselier damage model, Computer methods in applied mechanics and engineering, 192:107-124

[24] Jackiewicz, J. and Kuna, M. (2003) Non-local Regularization for FE Simulation of Damage in Ductile Materials, Computational Materials Science, 28:684-695

[25] Comi, C. and Perego, U. (2004) Criteria for Mesh Refinement in Nonlocal Damage Finite Element Analyses, European Journal of Mechanics A-Solids, 23:615-632

[26] Bazant, Z.P. and Jirasek, M., (2002) Nonlocal Integral Formulations of Plasticity and Damage: Survey of Progress, Journal of Engineering Mechanics-ASCE, 128:1119-1149

[27] Needleman, A. (1988) Material Rate-dependence and Mesh-sensitivity in Localization Problems, Computational Methods in Applied Mechanics and Engineering, 67:69-85

[28] Cockroft, M.G. and Latham, D.J. (1968) Ductility and the Workability of Metals, Journal of the Japan Institute of Metals, 96:33-39

[29] Ayada, M. and Higashino, T. and Mori, K. (1987) Central Bursting in Extrusion of Inhomogeneous Materials, Advanced Technology of Plasticity, Lange, K., Springer-Verlag, Berlin, 553-558

[30] Oyane, M. (1972) Criteria of Ductile Fracture Strain, Bulletin of JSME, 15:1507-1513

[31] Brozzo, P. and DeLuca, B. and Rendina, R. (1972) A New Method for the Prediction of the Formability Limits of Metal Sheets, 7th Biennial Conf. Int. Deep Drawing Research Group, Veerman, Chr., Amsterdam

[32] Gunawardena, S.R. and Jansson, S. and Leckie, F.A. (1991) Transverse ductility of metal matrix composites, Winter Annual Meeting of the American Society of Mechanical Engineers, Dec 1-6 1991, American Society of Mechanical Engineers, Aerospace Division (Publication) AD, Atlanta, GA, USA, Published by ASME, New York, NY, USA, 22:23-30

[33] Rice, J.R. and Tracey, D.M. (1969) On the ductile enlargement of voids in triaxial stress fields, Journal of the Mechanics and Physics of Solids, 17:201-217

[34] Hancock, J.W. and Mackenzie, A.C. (1976) On the mechanisms of ductile failure in high-strength steels subjected to multi-axial stress-states, Journal of the Mechanics and Physics of Solids, 24:147-169

[35] Drabek, T. (2005) Modeling of Matrix Damage in Particle Reinforced Ductile Matrix Composites, Ph.D. thesis, Technische Universitaet Wien

[36] Leblond, J. B. and Perrin, G. and Devaux, J. (1994) Bifurcation Effects in Ductile Metals with Nonlocal Damage, Journal of Applied Mechanics, 61:236-242

[37] Abaqus (2006) Users Manual, ABAQUS Inc

[38] Duan, X. and Jain, M. and Metzger, D. and Kang, J. and Wilkinson, D.S. and Embury, J.D. (2005) Prediction of shear localization during large deformation of a continuous cast AlMg sheet, Materials Science and Engineering A, A394:192-203

[39] Thomason, P. F., Ductile Fracture of Metals, Pergamon Press, Oxford, 1990

[40] Needleman, A. and Tvergaard, V. (1987) An analysis of ductile rupture modes at a crack tip, Journal of the Mechanics and Physics of Solids, 35:151-183

[41] Rousselier, G. (1987) Ductile fracture models and their potential in local approach of fracture, Nuclear Engineering and Design, 105:97-111

[42] LLorca J., and Needleman, A. and Suresh, S. (1991) An analysis of the effects of matrix void growth on deformation and ductility in metal-ceramic composites, Acta Metallurgica et Materialia, 39:2317-2335

[43] LLorca, J. and Segurado, J. (2004) Three-dimensional multiparticle cell simulations of deformation and damage in sphere-reinforced composites, Materials Science and Engineering, A365:267-274

[44] Enakoutsa, K. and Leblond, J.B. and Perrin, G. (2007) Numerical implementation and assessment of a phenomenological nonlocal model of ductile rupture, Computer Methods in Applied Mechanics and Engineering, 196:1946-1957

[45] Fischer, F.D. and Kolednik, O. and Shan, G.X. and Rammerstorfer, F.G. (1995) A Note on Calibration of Ductile Failure Damage Indicators, International Journal of Fracture, 73:345-357